Dalton Transactions

ROYAL SOCIETY OF CHEMISTRY

COMMUNICATION

View Article Online
View Journal | View Issue

Cite this: *Dalton Trans.*, 2024, **53**, 12460

Received 25th June 2024,
Accepted 11th July 2024

DOI: 10.1039/d4dt01835d

rsc.li/dalton

Reduction of hexaazatrinaphthylenes by divalent lanthanocenes leads to ligand-based multiconfigurational properties†

Siobhan R. Temple,[a] Jinkui Tang,[b] Graham J. Tizzard,[c] Akseli Mansikkamäki *[d] and Richard A. Layfield *[a]

Reduction of hexaazatrinaphthylene (HAN) and its hexamethyl derivative with $[Cp^*_2Sm(THF)_2]$ or $[Cp^*_2Yb(OEt_2)]$ produces $[(Cp^*_2Ln)_3(R_6HAN)]$ (Ln = Sm, Yb; R = H, Me), where the heterocyclic ligand forms as a trianion. The magnetism and electronic structure of these compounds reflect unusual multiconfigurational character within the reduced ligand but not the lanthanide ions.

N-Heterocycles based on hexaazatriphenylene (HAT, Scheme 1) attract interest owing to their proposed applications as organic materials, including liquid crystals, molecular recognition systems, non-linear optics, semiconductors and other electronic devices.[1] The redox-active nature of HAT and its derivatives also provides opportunities for developing new cathode materials in lithium-ion batteries.[2]

From a coordination chemistry perspective, the six nitrogen atoms in HAT-type complexes play a multifaceted role, allowing coordination of up to three metal centres and, in principle, enabling the injection of multiple electrons into the electron-deficient heterocycle.[3] For example, threefold reduction of the extended derivative hexaazatrinaphthylene (HAN, Scheme 1) by a magnesium(I) reagent produces a trimetallic complex of the $[HAN]^{3-}$ trianion, which adopts a spin state with $S = 1/2$ but with pronounced multiconfigurational and triradical character.[4] Although rare, transition metal,[5] lanthanide[6–8] and actinide[9] complexes of $[HAN]^{-}$ or $[HAN]^{3-}$ are of interest because the radical ligands can promote strong exchange coupling. In the case of the highly anisotropic lanthanides terbium and dysprosium, the radical character of the ligand has been shown to support single-molecule magnet (SMM) behaviour.[6]

In f-element HAN complexes, it is noteworthy that the ubiquitous reducing agent KC_8 is typically used to introduce radical character into the ligand. As an alternative approach, we were interested to explore the idea that lanthanide complexes of radical HAN ligands could be obtained by direct reduction of the heterocycle using divalent lanthanides. For this purpose, the divalent samarium and ytterbium metallocenes Cp^*_2Ln offer promise ($Cp^* = C_5Me_5$). Whereas the more strongly reducing Cp^*_2Sm is expected to convert HAN into its radical trianion,[10] the milder reducing agent Cp^*_2Yb offers the possibility of metal- and/or ligand-based multiconfigurational character, a phenomenon described by Andersen, Nocton *et al.* in related ytterbocene complexes of N-heterocyclic ligands.[11–15]

The target complexes $[(Cp^*_2Ln)_3(HAN)]$ ($\mathbf{1_{Ln}}$) and the hexamethyl analogues $[(Cp^*_2Ln)_3(Me_6HAN)]$ ($\mathbf{2_{Ln}}$) (Ln = Sm, Yb) were synthesized by adding $[Cp^*_2Sm(THF)_2]$ or $[Cp^*_2Yb(OEt_2)]$ to the corresponding pro-ligand, according to Scheme 2. The molecular structures of all four compounds were determined by X-ray crystallography and found to be similar (Table S1†). Only the structures of $\mathbf{1_{Sm}}$ and $\mathbf{1_{Yb}}$ are discussed in detail, with $\mathbf{2_{Sm}}$ and $\mathbf{2_{Yb}}$ shown in the ESI (Fig. S1 and S2†). The four compounds also have very similar FTIR spectra (Fig. S3†). The structures of $\mathbf{1_{Sm}}$ and $\mathbf{1_{Yb}}$ consist of a HAN ligand bound in a bidentate manner through the three coordination sites to

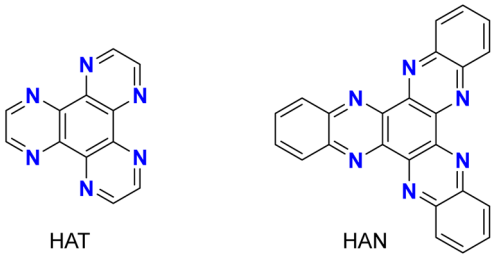

Scheme 1 Structures of hexaazatriphenylene (HAT) and hexaazatrinaphthylene (HAN).

[a]*Department of Chemistry, School of Life Sciences, University of Sussex, Brighton BN1 9QG, UK. E-mail: r.layfield@sussex.ac.uk*
[b]*Changchun Institute of Applied Chemistry, Chinese Academy of Sciences, Renmin Street 5626, 130022 Changchun, China*
[c]*School of Chemistry, University of Southampton, University Road, Southampton, SO17 1BJ, UK*
[d]*NMR Research Unit, University of Oulu, P.O. Box 8000, FI-90014, Finland. E-mail: akseli.mansikkamaki@oulu.fi*

†Electronic supplementary information (ESI) available: Synthesis details, spectroscopic characterization, magnetic measurements and computational details. CCDC 2331051–2331054. For ESI and crystallographic data in CIF or other electronic format see DOI: https://doi.org/10.1039/d4dt01835d

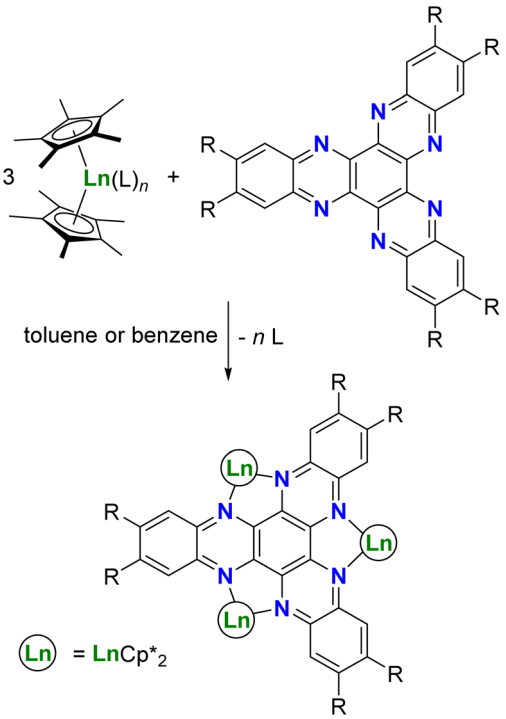

Scheme 2 Synthesis of $\mathbf{1}_{Ln}$ (R = H) and $\mathbf{2}_{Ln}$ (R = Me), where Ln = Sm with $(L)_n = OEt_2$, and Ln = Yb with $(L)_n = (THF)_2$.

three samarium or ytterbium atoms, respectively, in addition to two η^5-Cp* ligands per lanthanide (Fig. 1). A mirror plane coincident with atoms Sm2 or Yb2 lies perpendicular to the plane of the HAN ligand. In $\mathbf{1}_{Sm}$, the Sm–N distances lie in the range 2.426(4)–2.461(5) Å and the Sm–Cp* centroid distances are 2.4627(4) and 2.4630(4) Å for Sm1, and 2.4513(4) and 2.4708(4) Å for Sm2. The Cp*–Sm–Cp* bending angles are 141.12(1)° for Sm1 and 141.78(2)° for Sm2. The analogous Yb–N distances in $\mathbf{1}_{Yb}$ are shorter at 2.323(4)–2.365(5) Å, and the Yb–Cp* distances to Yb1 are 2.3517(3) and 2.3495(4) Å, and those to Yb2 are 2.3375(4) and 2.3528(4) Å. The Cp*–Yb–Cp* bending angles are narrower at 138.80(1) and 139.33(2)°.

The structural parameters determined for the four compounds suggest that threefold reduction of HAN to its trianionic form $[HAN]^{3-}$ has occurred, resulting in formal oxidation of all the lanthanide centres to the trivalent forms. Marked decreases in the Sm–Cp* distances from 2.5913(13) and 2.6006(12) Å in $[Cp^*_2Sm(THF)_2]$ are found in $\mathbf{1}_{Sm}$, consistent with a reduction in the ionic radius of samarium. Similarly, the Yb–Cp* distances of 2.420(2) Å and 2.409(3) Å in $[Cp^*_2Yb(OEt_2)]$ are substantially longer than those in $\mathbf{1}_{Yb}$, which are reminiscent of a well-defined ytterbium(III) metallocene such as $[Cp^*_2Yb(bipy)]^+$ (bipy = 1,2-bipyridyl).[14]

The ^{1}H NMR spectra of $\mathbf{1}_{Sm}$ and $\mathbf{2}_{Sm}$ in toluene-D_8 at 303 K confirm that the solid-state structures are preserved in solution (Fig. S4 and S5†). The HAN-ligated complex $\mathbf{1}_{Sm}$ shows a singlet at δ = 2.91 ppm for the Cp* methyl groups and resonances at −37.75 and −64.63 ppm for the HAN protons. The Me_6HAN-ligated complex $\mathbf{2}_{Sm}$ features resonances at δ = 3.00 ppm for the Cp* methyl groups, 33.50 ppm for the HAN methyl substituents, and −61.08 ppm for the HAN protons. The ^{1}H NMR spectra of $\mathbf{1}_{Yb}$ and $\mathbf{2}_{Yb}$ (Fig. S6 and S7†) also feature paramagnetically shifted resonances, further supporting the idea that the ytterbium centres have been oxidized from the diamagnetic, divalent form (with configuration $4f^{14}$) to the paramagnetic trivalent form (with configuration $4f^{13}$). The ^{1}H NMR spectrum of $\mathbf{1}_{Yb}$ displays resonances at δ = 93.38 and 0.37 corresponding to the two HAN proton environments, and at −2.57 ppm corresponding to the Cp* methyl groups. In the case of $\mathbf{2}_{Yb}$, the Cp* and HAN methyl groups were observed at δ = −2.91 and 92.86 ppm, respectively, whereas the HAN protons were not observed.

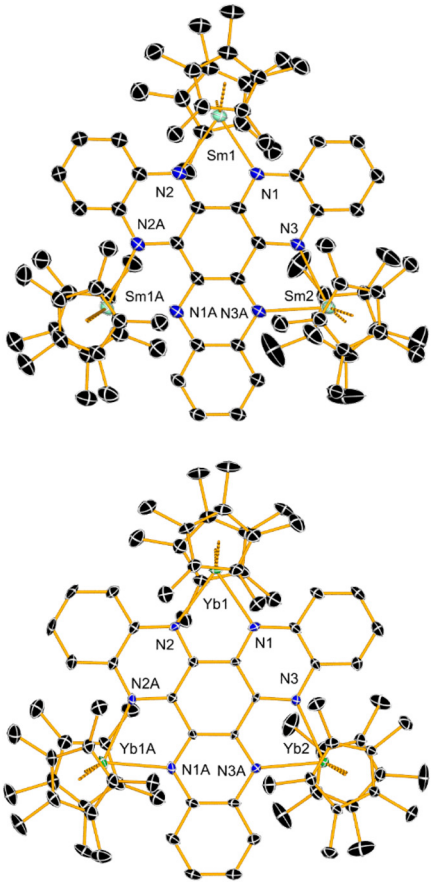

Fig. 1 Thermal ellipsoid representation of the molecular structures of $\mathbf{1}_{Sm}$ (30% probability) and $\mathbf{1}_{Yb}$ (50% probability). For clarity, hydrogen atoms are not shown.

Previous work by Andersen *et al.* has shown that the temperature dependence of the ^{1}H NMR chemical shift can indicate intermediate valence in N-heterocycle complexes of ytterbium metallocenes.[12,15] Therefore, the ^{1}H NMR spectra of the samarium and ytterbium compounds were examined at 213–373 K (Fig. S8–S15†). However, for all compounds, the ^{1}H NMR resonances show a near-linear temperature dependence, consistent with Curie–Weiss magnetic behaviour.

The UV/vis/NIR spectra of the four compounds in toluene (Fig. S16 and S17†) are strikingly similar and also reminiscent

of the spectrum of [(HAN){Mg(NacNac)}$_3$] (NacNac = *N*,*N*′-(2,6-diiso-propylphenyl)-3,5-dimethyldiketiminate), which consists of a well-defined $[HAN]^{3-}$ ligand with an $S = 1/2$ ground state. The spectra of $\mathbf{1_{Ln}}$ and $\mathbf{2_{Ln}}$ feature absorptions in the region 300–500 nm representing intra-ligand electronic transitions from lower lying doubly occupied molecular orbitals (MOs) and the singly occupied MO to the lowest unoccupied MO (LUMO). The absorptions at 900–1100 nm also appear to be characteristic of $[HAN]^{3-}$ in the spin doublet form (consistent with *ab initio* calculations, see below), and correspond to transitions from the highest occupied MO and the singly occupied MO to the LUMO.

Solid-state magnetic susceptibility measurements on $\mathbf{1_{Sm}}$ and $\mathbf{2_{Sm}}$ display non-Curie behaviour typical of samarium(III), which, as a single ion, has a $^6H_{5/2}$ ground state and a $^6H_{7/2}$ first-excited state approximately only 700 cm^{-1} higher in energy. For $\mathbf{1_{Sm}}$, the temperature-dependence of the molar magnetic susceptibility (χ_M), plotted as $\chi_M T$ *versus* temperature, shows a slightly non-linear increase from 0.15 cm^3 K mol^{-1} at 2 K to 1.80 cm^3 K mol^{-1} at 300 K (Fig. S18 and S19†). Very similar $\chi_M T(T)$ data were observed for $\mathbf{2_{Sm}}$, with the susceptibility continuing to increase above 300 K. The $\chi_M T(T)$ profile for $\mathbf{1_{Yb}}$ shows a steep increase in the susceptibility in the temperature range 2–25 K before increasing gradually to reach 6.34 cm^3 K mol^{-1} at 300 K (Fig. S20 and S21†). Compound $\mathbf{2_{Yb}}$ shows similar behaviour but with slightly lower values of $\chi_M T$. Whereas the behaviour of $\mathbf{1_{Sm}}$ and $\mathbf{2_{Sm}}$ is difficult to interpret using an empirical approach, the susceptibility of $\mathbf{1_{Yb}}$ and $\mathbf{2_{Yb}}$ suggest an exchange interaction since three Yb(III) ions and an $S = 1/2$ radical $[HAN]^{3-}$ ligand in an uncoupled system are expected to have a $\chi_M T$ value around 8.0 cm^3 K mol^{-1}, which is not observed and could be partly due to crystal field effects. Therefore, to gain further insight into their electronic structure, $\mathbf{1_{Sm}}$ and $\mathbf{1_{Yb}}$ were examined using density functional theory (DFT) and multireference calculations.

It has previously been shown that the $[HAN]^{3-}$ anion has close-lying doublet and quartet spin states, either of which can be the ground state depending on the conditions (Fig. 2).[4] The doublet states can also show multireference character. The energy difference between the spin doublet and quartet states in $\mathbf{1_{Sm}}$ and $\mathbf{1_{Yb}}$ can be estimated independently of the Ln–HAN interaction using DFT and 4f-in-core pseudopotentials.[16,17] In both cases, the quartet state is predicted as the ground state with the doublet state lying 590 cm^{-1} and 599 cm^{-1} above the ground state in $\mathbf{1_{Sm}}$ and $\mathbf{1_{Yb}}$, respectively. Based on the $\langle S^2 \rangle$ expectation values (Table S2†), the doublet states also show significant multireference character. This means that the DFT description of energy difference is not necessarily reliable, and once the 4f shells and the lanthanide–HAN exchange interaction is considered, the quartet state is no longer predicted as the ground spin state of the $[HAN]^{3-}$ ion.

The lanthanide–HAN interaction was studied in more detail by multireference calculations at the NEVPT2//SA-CASSCF level[18–21] using the Orca code.[22] The calculations explicitly correlated the 4f electrons of one lanthanide ion in $\mathbf{1_{Sm}}$ and $\mathbf{1_{Yb}}$ and three electrons of the $[HAN]^{3-}$ anion. Both structures

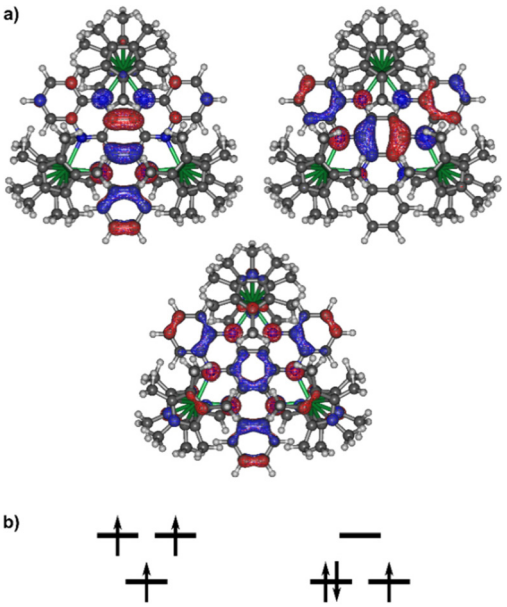

Fig. 2 (a) The three molecular orbitals in $\mathbf{1_{Yb}}$ occupied by the unpaired electrons of the $[HAN]^{3-}$ ligand. (b) Qualitative energy level diagram showing the occupations of the orbitals in the ligand quartet (left) and doublet (right) spin states.

contain two crystallographically inequivalent lanthanide centres. It should be noted that the three-electron-in-three-orbitals description of $[HAN]^{3-}$ does not provide an accurate description of the electron correlation effects within the full conjugated π-system; however, it is the largest active space that provides a balanced treatment of the correlation effects and remains computationally tractable. Due to the missing correlation effects in the π-system, the NEVPT2 correction leads to a reordering of the states (Tables S3–S6†), which is not desirable when the correction is only included up to second order. Thus, the results should be interpreted qualitatively.

The energy level structure of $\mathbf{1_{Yb}}$ is simpler than that of $\mathbf{1_{Sm}}$. Before the inclusion of spin–orbit coupling (SOC), the ground manifold of $\mathbf{1_{Yb}}$ consists of seven spin singlet states and seven spin triplet states. The manifold is spread over roughly 1000 cm^{-1} and is well-separated from the next excited manifold of states. The energy level structure is consistent with the Yb(III) ground ^2F term with a sevenfold orbital degeneracy being coupled to a $[HAN]^{3-}$ spin doublet with no orbital degeneracy. The ground state is a spin singlet and the first excited state is a spin triplet 9.5 cm^{-1} or 17 cm^{-1} above the ground singlet for Yb1 and Yb2, respectively (Table S6†). This implies that the lanthanide–HAN exchange interaction is weakly antiferromagnetic.

Once SOC is introduced, the ground manifold consists of 16 states spread over 700 cm^{-1} (Table S8†), consistent with the coupling of the Yb(III) $^2F_{7/2}$ ground multiplet with a $[HAN]^{3-}$ spin doublet. The SOC eigenvalues consist of weakly split quartets. Each quartet can be assigned to the coupling between a Yb(III) Kramers doublet and the $[HAN]^{3-}$ spin doublet. The

splitting of the states in the ground quartet of Yb1 is 0.0 cm^{-1}, 5.5 cm^{-1}, 6.2 cm^{-1} and 12.8 cm^{-1}, and in Yb2 it is 0.0 cm^{-1}, 9.8 cm^{-1}, 10.5 cm^{-1} and 10.9 cm^{-1}. The exchange coupling is relatively weak, but due to the non-axiality of the states, it cannot be simply mapped to an effective Lines exchange coupling constant.

In $\mathbf{1_{Sm}}$, before the inclusion of SOC, the ground manifold consists of two spin pentet and two spin septet states separated by roughly 300 cm^{-1} (Table S5†), consistent with an Sm (III) spin sextet state coupled to a $[HAN]^{3-}$ spin doublet state. The ground spin state is a pentet, again indicating antiferromagnetic metal–ligand exchange coupling. However, the presence of only two states of each spin multiplicity in the ground manifold is not consistent with the elevenfold orbital degeneracy of the Sm(III) ground ^6H term. The excited states above 300 cm^{-1} do not form any clearly separated manifolds that could be mapped to the interaction of the ^6H term with a spin doublet. This most likely indicates that the crystal-field splitting of the ^6H term is stronger than the energy separation between low-lying excited $[HAN]^{3-}$ doublet spin states, broadly consistent with the unusual $\chi_M T(T)$ data. Indeed, a clearly separate manifold of 88 states consisting of 44 pentet and 44 septet states spread over 1900 cm^{-1} can be identified from the energy level structure. This set can arise from the interaction of ^6H term with four $[HAN]^{3-}$ spin doublet states, which can be formed from the three electrons in the three $[HAN]^{3-}$ orbitals. Once SOC is introduced, the ground manifold is again a quartet with an energy spread of 0.0 cm^{-1}, 1.8 cm^{-1}, 11.3 cm^{-1} and 11.5 cm^{-1} in the case of both ions (Table S7†). The structure is more axial than in $\mathbf{1_{Yb}}$, but still shows significant splitting of quasi-doublets. The exchange coupling is again weak and cannot be mapped to a Lines-type exchange coupling constant.[23]

In conclusion, Cp^*_2Sm and Cp^*_2Yb reduce HAN and Me_6HAN to their trianionic forms to give the trimetallic complexes $[(Cp^*_2Ln)_3(HAN)]$ ($\mathbf{1_{Ln}}$) and $[(Cp^*_2Ln)_3(Me_6HAN)]$ ($\mathbf{2_{Ln}}$). For $\mathbf{1_{Yb}}$ and $\mathbf{2_{Yb}}$, the computational results provide evidence of the remarkable sensitivity of the $[HAN]^{3-}$ spin state to the local environment. Evidently, even a weak exchange interaction with lanthanide ions can lead to complicated mixing of lanthanide crystal-field states and multiple excited spin states of $[HAN]^{3-}$. This interplay of spin states means that the coordination chemistry of $[HAN]^{3-}$ radicals offer unique possibilities for designing molecular magnets, such as SMMs, in which ligand-based multiconfigurational character plays a prominent role.

Conflicts of interest

There are no conflicts to declare.

Acknowledgements

We acknowledge support from the University of Sussex, EPSRC (EP/V003089/1, EP/X036626/1), the National Natural Science Foundation of China (92261103), the Academy of Finland (332294), the University of Oulu (Kvantum Institute). Computational resources were provided by CSC-IT Center for Science in Finland and the Finnish Grid and Cloud Infrastructure (persistent identifier urn:nbn:fi:research-infras-2016072533).

References

1 J. L. Segura, R. Juárez, M. Ramos and C. Seoane, *Chem. Soc. Rev.*, 2015, **44**, 6850.
2 C. Peng, G.-H. Ning, J. Su, G. Zhong, W. Tang, B. Tian, C. Su, D. Yu, L. Zu, J. Yang, M.-F. Ng, Y.-S. Hu, Y. Yang, M. Armand and K. P. Loh, *Nat. Energy*, 2017, **2**, 17074.
3 S. Kitagawa and S. Masaoka, *Coord. Chem. Rev.*, 2003, **246**, 73.
4 J. O. Moilanen, B. M. Day, T. Pugh and R. A. Layfield, *Chem. Commun.*, 2015, **51**, 11478.
5 (*a*) J. O. Moilanen, N. F. Chilton, B. M. Day, T. Pugh and R. A. Layfield, *Angew. Chem., Int. Ed.*, 2016, **55**, 5521; (*b*) I. M. Piglosiewicz, R. Beckhaus, G. Wittstock, W. Saak and D. Haase, *Inorg. Chem.*, 2007, **46**, 7610.
6 C. A. Gould, L. E. Darago, M. I. Gonzalez, S. Demir and J. R. Long, *Angew. Chem., Int. Ed.*, 2017, **56**, 10103.
7 P. Zhang, Q.-C. Luo, Z. Zhu, W. He, N. Song, J. Lv, X. Wang, Q.-G. Zhai, Y.-Z. Zheng and J. Tang, *Angew. Chem., Int. Ed.*, 2023, **62**, e202218540.
8 R. Grindell, V. Vieru, T. Pugh, L. F. Chibotaru and R. A. Layfield, *Dalton Trans.*, 2016, **45**, 16556.
9 L. Barluzzi, S. P. Ogilvie, A. B. Dalton, P. Kaden, R. Gericke, A. Mansikkamäki, S. R. Giblin and R. A. Layfield, *J. Am. Chem. Soc.*, 2024, **146**, 4234.
10 W. J. Evans, S. L. Gonzales and J. W. Ziller, *J. Am. Chem. Soc.*, 1994, **116**, 2600.
11 M. Tricoire, N. Mahieu, T. Simler and G. Nocton, *Chem. – Eur. J.*, 2021, **27**, 6860.
12 C. H. Booth, M. D. Walter, D. Kazhdan, Y. J. Hu, W. W. Lukens, E. D. Bauer, L. Maron, O. Eisenstein and R. A. Andersen, *J. Am. Chem. Soc.*, 2009, **131**, 6480.
13 M. Schultz, J. M. Boncella, D. J. Berg, T. Don Tilley and R. A. Andersen, *Organometallics*, 2002, **21**, 460.
14 M. D. Walter, D. J. Berg and R. A. Andersen, *Organometallics*, 2006, **25**, 3228.
15 C. H. Booth, D. Kazhdan, E. L. Werkema, M. D. Walter, W. W. Lukens, E. D. Bauer, Y.-J. Hu, L. Maron, O. Eisenstein, M. Head-Gordon and R. A. Andersen, *J. Am. Chem. Soc.*, 2010, **132**, 17537.
16 M. Dolg, H. Stoll, A. Savin and H. Preuss, *Theor. Chim. Acta*, 1989, **75**, 173.
17 D. Andrae, U. Häußermann, M. Dolg, H. Stoll and H. Preuß, *Theor. Chim. Acta*, 1990, **77**, 123.
18 P. Siegbahn, A. Heiberg, B. Roos and B. Levy, *Phys. Scr.*, 1980, **21**, 323.
19 B. O. Roos, P. R. Taylor and P. E. M. Siegbahn, *Chem. Phys.*, 1980, **48**, 157.

20 P. E. M. Siegbahn, J. Almlöf, A. Heiberg and B. O. Roos, *J. Chem. Phys.*, 1981, **74**, 2384.
21 C. Angeli, R. Cimiraglia and J.-P. Malrieu, *J. Chem. Phys.*, 2002, **117**, 9138.
22 F. Neese, F. Wennmohs, U. Becker and C. Riplinger, *J. Chem. Phys.*, 2020, **152**, 224108.
23 L. F. Chibotaru, L. Ungur and A. Soncini, *Angew. Chem., Int. Ed.*, 2008, **47**, 4126.